ANALYSIS OF MICRODAMAGE IN THERMALLY
AGED CF/POLYIMIDE LAMINATES

J. Varna[*] **and H. Zrida**

Keywords: *Monte Carlo simulation, thermal aging, thermal cycling, tensile tests, intralaminar cracking*

Microdamage in the layers of CF Thornel® T650 8-harness satin-weave composites with a thermosetting NEXIMID® MHT-R polyimide resin, designed for high service temperatures, is analyzed. After cooling down to room temperature (RT), a multiple intrabundle cracking due to tensile transverse thermal stresses was observed in the $[(+45/-45)/(90/0)]_{2s}$ laminates studied. Then, the composite was subjected to two ramps of thermal cycling quantifying the increase in crack density in its layers. A comparison of two ramps with the same lowest temperature showed that the highest temperature in the cycle where thermal stresses were low had a significant detrimental effect on the thermal fatigue resistance of the composite. The effect of holding it at 288°C for 40 days was also studied: many new cracks formed in it after cooling down to RT. During the time at the high temperature, the mechanical properties degraded with time, and the crack density versus aging time was measured at RT. Then, both aged and nonaged specimens were tested in uniaxial quasi-static tension quantifying the damage development in layers of different orientation. Cracking in the layers was analyzed using fracture mechanics arguments and probabilistic approaches: a) a simple one, not considering crack interaction; b) Monte Carlo simulations. It is shown that cracking in the off-axis layers which are not in contact with the damaged 90°-layer can be predicted based on the Weibull analysis of the 90°-layer, whereas in the off-axis layer contacting the 90°-layer, the crack density is much higher due to the local stress concentrations caused by cracks in the 90°-layer. The thermal treatment degraded the cracking resistance in the surface and adjacent layer, whereas the composite close to the midplane was not changed.

Deppartment. of Engineering Sciences and Mathematics, Lulea University of Technology Lulea, Sweden
[*]Corresponding author; e-mail: Janis.Varna@LTU.SE

1. Introduction

The increasing interest of aerospace industry in composite materials for applications in harsh environments has been driving the improvement and development of new composites. The composites intended for aero-engine applications, which are considered in the current paper, are designed to work at high temperatures. A long exposure of composites to elevated temperatures can cause irreversible changes (thermal aging in this paper) in their morphology reducing the strength and stiffness [1-3]. In addition, cyclic variations between high and low temperatures can lead to fatigue resulting in microdamage accumulation [4-6]. The effect of thermal cycling between –100°C and 100°C, as well as thermal aging for 250h and, 400h at 110°C, on the mechanical performance of carbon fiber/RTM6 resin and carbon fiber/BMI resin cross-ply laminates was studied in [4], showing that, due to matrix and interface degradation, the intralaminar crack density is a clear function of aging time,

The elevated temperature level during thermal cycling with a fixed lowest temperature has an accelerating effect on the microdamage development [5]. At the highest temperature in the cycle, the composite laminate is close to the stress-free state, and, therefore, a thermoelastic analysis and stress-based failure criteria cannot explain the degrading role of the highest temperature in the damage development.

In the Paris-type rule for a crack growth analysis in thermal cycling, the crack growth rate is a power function of change in the energy release rate (ERR) in the cycle. The ERR is highest at the lowest temperature in the cycle and lowest at the highest temperature. Therefore, at fixed lowest temperature, an increase in the highest temperature lead to great variations in the ERR. Nevertheless, this feature alone cannot explain this effect, and there have to be other reasons, for example, during exposure to a high temperature, irreversible phenomena can take place and a microcrack grows when the lowest temperature in the cycle with the high stress is reached. The possible causes for the degradation are disintegration of the molecular network, leading to the degradation of resin properties, including the resistance to crack growth. In [3], authors demonstrated that this effect can be intensified and accelerated if an elevated pressure is added.

The study performed in [7] on the behavior of an IMS/977-2 carbon fiber/epoxy composite at 217°C showed that the time at an elevated temperature affects its viscoelastic properties. This can be explained by a change in the glass-transition temperature. The chemical and physical processes occurring during aging are accompanied by a change in the molecular mobility — the glass-transition temperature increases at the beginning of aging and then decreases.

The degradation of a neat polyimide resin and a CF/polyimide composite at 320 and 360°C was studied in [8], proving that the composite weight loss during aging was caused by matrix degradation, whereas carbon fibers in the composite showed a good thermal oxidation resistance. A development of high-temperature polymeric resins was reported in [9], where the common epoxy with a limiting service temperature of 135°C was replaced by a polyimide resin for service temperatures between 250 and 350°C.

The objective of the present paper is to report recent results on the development of high-temperature polyimide-based composites and to analyze their resistance to intrabundle cracking. Some intrabundle cracks appeared in all layers already at the end of the manufacturing cycle, when the composite was cooled down to room temperature (RT). The increase in crack density when composites are subjected to great temperature variations (thermal cycling) and exposed to high long-duration temperatures (thermal aging) is studied. During the high-temperature exposure, the cracking resistance of the aged composite is degraded, and in the following mechanical tensile loading, more cracks are created in the aged composite than in the nonaged one. An analysis of differences in the cracking and delamination growth in as manufactured (called "nonaged" (NA)) and an "aged" ("A") woven quasi-isotropic carbon fiber/polyimide composite is performed. The cracking initiation and growth of microcracking is analyzed using the statistical approach based on the Weibull distribution of the initial strength and fracture mechanics, focusing on differences in the growth of crack density in different layers.

2. Experiments

2.1. Description of the composite

A quasi-isotropic $[(+45/-45)/(90/0)]_{2s}$ composite was manufactured by Resin Transfer Molding (RTM) using a Cytec T650 CF 8-harness satin weave and a thermosetting polyimide resin, denoted asNEXIMID® MHT-R (MHT-R). This binder was provided as a low-molecular-weight phenylethynyl terminated polyimide resin containing a combination of 4-(phenylethynyl)phthalic anhydride (4-PEPA), an end-group cross-linker, and ethynyl bis-phthalic anhydride (EBPA) as the main chain cross-linker. The composite was cured at 340°C for 30 min, followed by a 2.5-h postcure at 370°C under a 12-bar pressure. Thereafter, the plate was slowly cooled down to 0°C and then heated back to room temperature (RT). The cooling to 0°C was to introduce thermal stresses higher than those at RT, expecting that the microdamage state introduced will not be sensitive to small temperature variations when composite is used at RT. In what follows, this damage state is called the "initial damage state," indicating that this is the damage existing before any treatment. In figures, the composite is labelled as "432 plate".

The volume fraction of fibers in the composite was about 60%. Some mechanical properties of the T650/MHT-R quasi-isotropic laminate and the manufacturing details are given in [10]. The composite exists only as a quasi-isotropic woven laminate, and therefore the properties of the unidirectional composite that would be useful for modeling were not available. They were estimated by a back-calculation from the measured elastic constants of the woven composite, from typical CF/EP data, and from fiber data:

$$E_1 = 141.0 \text{ GPa}, \ E_2 = 8.8 \text{ GPa}, \ v_{12} = 0.27, \ v_{23} = 0.44,$$

$$G_{12} = 3.6 \text{ GPa}, \ G_{23} = 3.1 \text{ GPa}, \ \alpha_L = 0, \ \alpha_T = 25 \cdot 10^{-6} \ 1/°C.$$

The average thickness of one bundle was approximately 0.18 mm. The bundle width was about 1.5 mm, and the high width-to-thickness ratio partially justified the "layer assumption" used to estimate the stress state by the FEM in the central part of the bundle, which was far from the interface with the resin region between bundles. Hence, in analyzing the thermal stress state at the specimen edge, the 8-harness satin mesoarchitecture of the composite was approximated by a laminate with "layers" of corresponding fiber orientation.

Specimens with dimensions 150 × 12 mm were cut from each plate. Their edges were first polished using sand papers (P240, P600, P1200, P2500, and P4000) and then a diamond slurry (from 9 to 0.25 mμ). Part of the specimens were labelled with the letter "A" and subjected to isothermal aging at 288°C for 960 h (40 days) in an air environment. After certain hours of aging, they were cooled down to RT for damage quantification.

2.2. Experimental procedures

Two types of tests were performed on aged and nonaged specimens: thermal cycling and tensile loading–unloading ramps with an increasing maximum strain in the ramps.

Two different thermal cycling ramps were used. In ramp R1, the temperature was varied between –60°C and RT, but in ramp R2, — between –60°C and 288°C. Specimens were first exposed to each temperature for 10 minutes. The maximum number of loading cycles was 150.

The tensile loading and unloading tests with an increasing maximum stress were performed at RT with a displacement rate of 2 mm/min. The strains were measured by an extensometer with a gage length of 50 mm.

The damage state in all specimens was analyzed as a function of aging time using an optical microscope. Edge inspections were performed after a certain number of cycles in the thermal fatigue and after each loading-unloading step in the

tensile loading. In each layer, the number of cracks N_i over a distance L (50 mm) on the specimen edge was counted, and the crack density was estimated as

$$\rho_i = \frac{N_i}{L \sin \theta_i},$$ (1)

where θ_i is the fiber orientation angle in an ith layer. In Eq. (1), $\sin \theta_i$ is introduced to ensure that the distance between cracks in a layer is determined perpendicularly to the crack plane and not along the specimen edge.

The void content was defined as the area fraction of voids on the edge surface and was measured using an image analysis software (NIS-elements BR) together with an optical microscope. The average void content was measured on an area of about 100 mm². From one specimen to another, the average void content varied from 0.3 to 2.4%, which is a very high variability between specimens. Most of the NA 90°-layer edge cracks existing before testing were linked with interbundle voids. The role of voids is dual: they act as stress concentrators, and therefore first cracks appear at a relatively low average thermal stress, but they also lead to greater relaxation of local stresses after a crack is created, delaying the origination of new cracks in this location and arresting the growth of existing cracks; see [11, 12] for mechanical loading cases.

3. Results and Discussion

3.1. Initial damage state

The initial damage state corresponds to the thermal stresses at 0°C reached during the last part of the manufacturing cycle (the temperature difference between the cross-linking temperature, which was assumed to be stress-free, was $\Delta T = -340$°C). The thermal stress state in the bulk part of a bundle with a high width to thickness ratio can be roughly estimated using the Classical Laminate Theory (CLT). According to the CLT, in a quasi-isotropic laminate, the thermal stresses transverse to the fiber direction are the same in all layers, and the in-plane shear stress is zero. Hence, the number of initiated cracks statistically should be the same in all layers. This conclusion corresponds to an infinite composite plate.

 In contrast to the central part of a plate, where the CLT solution for laminates is valid, in a specimen cut from the central part of the plate, the stress state is different: the specimen has free edges, where the stress state is 3-D. It was observed that, on the specimen edge, the crack density in different layers was different: the highest crack density was in the surface +45°-layers; it was lower in the 90°-layers, but still higher than in the internal ±45°-layers, where it was very low.

It has to be mentioned that care was taken to ensure that the cutting itself did not introduce damage: after cutting, about 1 mm of the material from each edge was removed by a fine polishing. Anyway, cutting problems cannot explain the systematic difference between the crack densities in layers of different orientation.

To explain the cracking features observed, a 3-D FEM analysis of thermal stresses was performed to clear up the effect of free edge on the distribution of thermal stresses. A $[(+45/-45)/(90/0)]_{2s}$ laminate was modeled assuming that the bundle mesostructure can be homogenized and using the values of thermoelastic constants of the CF UD composite given in Sect. 2.1. Results for a 4-mm-wide specimen showed that, even for narrow specimens, the local transverse stress in the middle between edges was similar to that given by the CLT, proving that, for this geometry, the stress perturbations from both edges did not overlap and the magnitude of edge effect was not affected by the other edge. The local in-plane shear stress in an off-axis layer at the edge was not zero, but still it was significantly lower than the transverse stress, and its effect on the cracking could be assumed small. Clear differences between the transverse edge stresses in the ±45°- and 90°-layers were found. In the 90°-layers, the transverse edge stress was by about 20% higher, whereas in all 45°-layers, it was approximately 30% of the CLT stress. Thus, after cutting, the thermal stress state at the specimen edge was different from that in the corresponding part of the "infinite "plate.

At the 90°-layer edge, the transverse stress had increased by 20% compared with that before cutting. However, the cutting was performed at RT, which was about 22°C higher than the lowest temperature during the manufacturing cycle re-

sponsible for the damage state observed, and the thermal stresses in bundles had lowered by about 6-7% relative to the stress state at 0°C. The 20% increase in stresses at the edge was a much greater change than the reduction in the thermal stress when the plate was brought from 0°C to RT. This means that, in the edge region of the 90°-layer of the finite specimen, new cracks had been created. It is not a priori clear, whether these new cracks had grown inside the specimen because of the following two reasons: a) the stress away from edges did not change when cutting the specimen, and the stress there was lower than at the edge; b) the propagation of an initiated crack along fibers requires a different level of stress than the initiation one. The initiation- propagation problem will be considered throughout this paper. The experiments performed showed that, for our material, the stress level for crack propagation was lower than the initiation stress. Therefore, it is very probable that the new 90°-cracks initiated at the specimen edge propagated as tunnels through the whole specimen even if the stress in the middle part of the 90°-layer was lower.

According to FE results, the local transverse stress in the edge region of 45°-layers was much lower than in the middle part, which means that new cracks were not introduced in these layers by making specimens. If this analysis is correct, the crack density on the edge of the 45°-layers was equal to the crack density in the middle part of these layers (new cracks had not been created, and the number of cracks on the edge could not be lower than in the same place before cutting the specimen). Then, according to the previous paragraph, the crack density in the middle part of the 90°-layer was higher than that observed on the edge of the 45°-layer.

To explain the much higher initial crack density in the surface layers, we have to distinguish two phases in evolution of an individual crack: initiation and propagation along fibers.

The initiation is a very complex process: cracks initiate because of stress concentrations in places where the local fiber content due to clustering is high and/or because the fiber/matrix interface or the matrix in these regions is "imperfect" owing to impregnation problems. Adding to this description the stress concentrations from randomly distributed voids, we see that the crack initiation process is stochastic and starts by coalescence of fiber/matrix debonds, leading to the creation and growth of a "defect" in the ply thickness direction. After reaching a certain size, this growth becomes unstable and finally slows down close to the interface with the next layer.

The initial part of the sequence of growth of events in the thickness direction is controlled by the ply- scale thermal stress σ_T in the corresponding location, which, according to the CLT, is the same for all layers. Hence, the CLT cannot explain why cracking in the surface layer is different. However, in the final part of the initiation process, the coalesced debonds (large created defects) start to grow in the layer thickness direction as a crack. According to the Linear Elastic Fracture Mechanics (LEFM), the stress required for an internal crack to grow is higher than that for a crack of the same size connected to the free surface. This result is well known in the LEFM for a crack of size a in an infinite plate and a crack of the same size starting from the surface of a semi-infinite plate [13]. In this paper, we call this stress level the "initiation stress."

Therefore, the conditions for crack initiation in the surface and internal layers are different: at a given transverse stress σ_T for a defect of given size at the free surface, the ERR for growth in the ply thickness direction is higher than that for a defect in the internal region. In [14], the following relationship between crack initiation stresses in the internal and surface layers of the same orientation was suggested:

$$\sigma_{T,init}^{internal} = k\sigma_{T,init}^{surface},$$

where $k = 1.12\sqrt{2}$.

The initiation of a crack at a certain stress is a stochastic process with a certain probability and random location. In simulations of crack initiation, we assume that the layer in its transverse direction can be considered as consisting of a chain of elements. Each element has its individual strength, but altogether, the transverse strength of elements follows the two-parameter Weibull strength distribution

$$P_f = 1 - \exp\left[-\left(\frac{k\sigma_T}{\sigma_{in0}}\right)^m\right], \tag{2}$$

where $k = 1.12\sqrt{2}$ for the surface layer and $k = 1$ for an internal layer. Location of an element with a certain strength is random. The parameter k is introduced into Eq. (2) to reflect the favorable situation for crack initiation in the surface layer of laminate.

According to Eq. (2), at a given stress (given temperature in the case of thermal stress), the probability of element failure is much higher, and there are many more initiated cracks in the surface layer of a quasi-isotropic laminate than in its internal layers.

When the crack becomes sufficiently large in the ply thickness direction (this size is limited: it cannot be larger than the ply thickness), the propagation of the initiated crack along the fiber direction in the layer becomes energetically possible. The propagation of a crack may be described by the LEFM, which states that a crack will propagate when the potential energy release rate (ERR) G reaches or exceeds a critical value G_c. Usually, the analysis is performed for a homogenized layer neglecting the fiber/matrix microstructure. We call the corresponding stress level the "propagation stress." The available energy is a quadratic function of stress level and depends on ply thickness (in our case, the thickness is the same for all layers) and position of the layer: in the surface layer, it is about 2.4 times larger than in an internal one [15]. Hence, the propagation of an initiated crack in the surface layer can start at much lower thermal stresses. Summarizing the previous discussion, we conclude that: a) the number of initiated cracks in the surface layer at RT is higher; b) the propagation of initiated cracks in the surface layer require a much lower stress than for cracks in the internal layers. Therefore, the crack density in the surface layers at RT is much higher.

3.2. Thermal fatigue

Each data point for crack density in Fig. 1 corresponds to the average on two edges of one specimen for all layers of given orientation (the surface layers are analyzed separately). Since different specimens were used for different numbers of cycles N, the crack density at a greater N is sometimes lower that for smaller N. For all layer orientations, the R2 ramp (−60°C to 288°C) induced more damage than R1 (−60°C to RT). This means that not only the lowest temperature during the cycle, but also the temperature interval $\Delta T = T_{\min} - T_{\max}$ at a fixed $T_{\min}$ affects the cracking in thermal cycling. This conclusion is consistent with the Paris law for the growth of an individual crack in cyclic loading, which states that the crack growth rate is a power function of difference in the ERR (validated in [16]): ΔG is larger for the R2 ramp than for the R1 ramp (because of the larger range of stress changes between the max and min temperatures):

$$\frac{da}{dN} = A\Delta G^{\beta}, \quad \Delta G = G(T_{\min}) - G(T_{\max}). \tag{3}$$

The parameters A and b in Eq. (3) are expected to be material-system-dependent and can be affected by exposure to high a temperature. The crack density in thermal cycling is highest in the surface layers, lower in the 90°-layer, and still lower in the internal 45°-layers. A much higher crack density in the surface layers was also observed in [17], where a thermal cycling to cryogenic temperatures was performed. In [17], the crack density determined on the edge of the 90°-layer was also higher than on edges of the internal 45°-layers.

To explain the cracking behavior observed, we have to recall that, in fatigue, a certain number of cycles N_{init} is required to initiate a crack and a different number of cycles N_{prop} is required for its propagation along fibers. If $N_{\text{prop}} \gg N_{\text{init}}$, the "individual fatigue life" (the number of cycles for a full development of the crack through the specimen) is propagation-governed; in contrary, if $N_{\text{init}} \gg N_{\text{prop}}$, the cracking in fatigue is initiation-governed.

As already mentioned in Sect. 3.1, the initiation is a stochastic process with a certain probability. A generalization of the Weibull model (2) for crack initiation in cyclic loading is suggested in [16, 17], where some experimental support is also presented.

If the crack density in a kth layer is low enough to allow for large plateau regions in the stress distribution between cracks, the stress level for a next crack mostly depends on the strength in this location and only marginally on the stress perturbations caused by the cracks created earlier. In this case, the probability of failure as a function of the transverse stress can be estimated using the formula
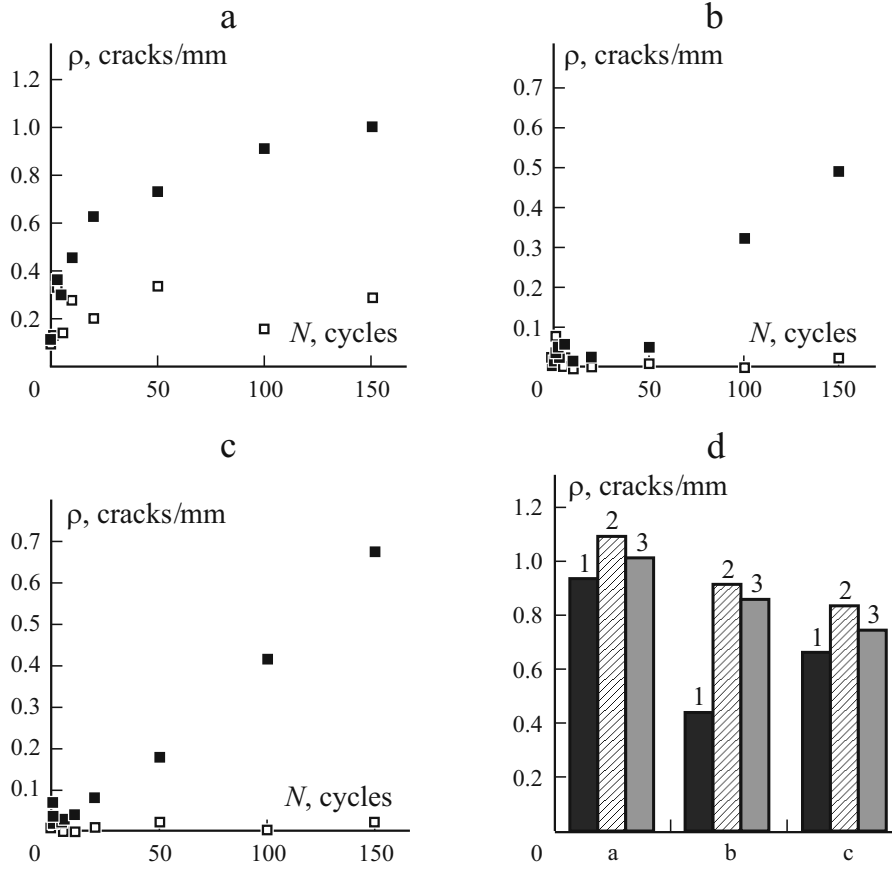
$$P_f = \frac{\rho_k(\sigma_{\text{T}})}{\rho_{k,\max}}. \tag{4}$$

Fig. 1. Crack density ρ on the edge of the surface 45°-layer (a) , internal ±45°-layers (b), and 90°-layers (c) vs. the number N of thermal fatigue cycles in ramps R1 (–60-RT°C) (□) and R2 (–60-288°C) (■), and in the same layers after 150 cycles in R2 ramps vs. the distance $d = 0$ (1), 0.9 (2), and 2.4 mm (3) from edge.

In Eq. (4), $\rho_{k,\max}$ is the maximum possible crack density in a layer corresponding to the so-called "characteristic damage state." Based on experimental observations, $\rho_{k,\max} \approx 1/t_k$, where t_k is thickness of the layer [15]. The expression for the initiated crack density in cyclic loading reads

$$\frac{\rho_k(\sigma_{\mathrm{T}}, N)}{\rho_{k,\max}} = 1 - \exp\left[-N^\alpha \left(\frac{k\sigma_{\mathrm{T}}}{\sigma_{\mathrm{in0}}}\right)^m\right]. \tag{5}$$

The density of initiated cracks in Eq. (5) depends on the parameter k, which, due to the higher significance of surface defects, is greater for surface layers.

To investigate whether edge cracks propagate inside the specimen, the edge of specimen 432-18, subjected to 150 cycles in R2, was polished to quantify the damage state at a distance d from the specimen edge ($d = 0.9$ and 2.4 mm). The results obtained are presented in Fig. 1d and indicate that the value of ΔG was sufficient for cracks to reach, in 150 cycles, the edge of all layers, except the internal 45°-layers. To illustrate this, let us denote by ΔG_{90} the available value of ΔG in the middle part of the 90°- and all internal 45°-layers. According to Sect. 3.1, $\Delta G = 2.4\Delta G_c$ in the middle of the surface 45°-layer and $\Delta G = 2.4 \cdot 0.3^2 \Delta G_{90} \approx 0.22\Delta G_{90}$ at the edge of this layer (see the discussion about edge stresses in Sect. 3.1). Nevertheless, according to Fig. 1d, the value of ΔG was sufficiently great for all cracks to reach the edge of the surface layer in $N = 150$ cycles. In contrary, $\Delta G = 0.3^2 \Delta G_{90}$ in the internal 45°-layers at the edge which, according to Fig. 1d, had not been sufficient for all cracks to reach the edge in 150 cycles.
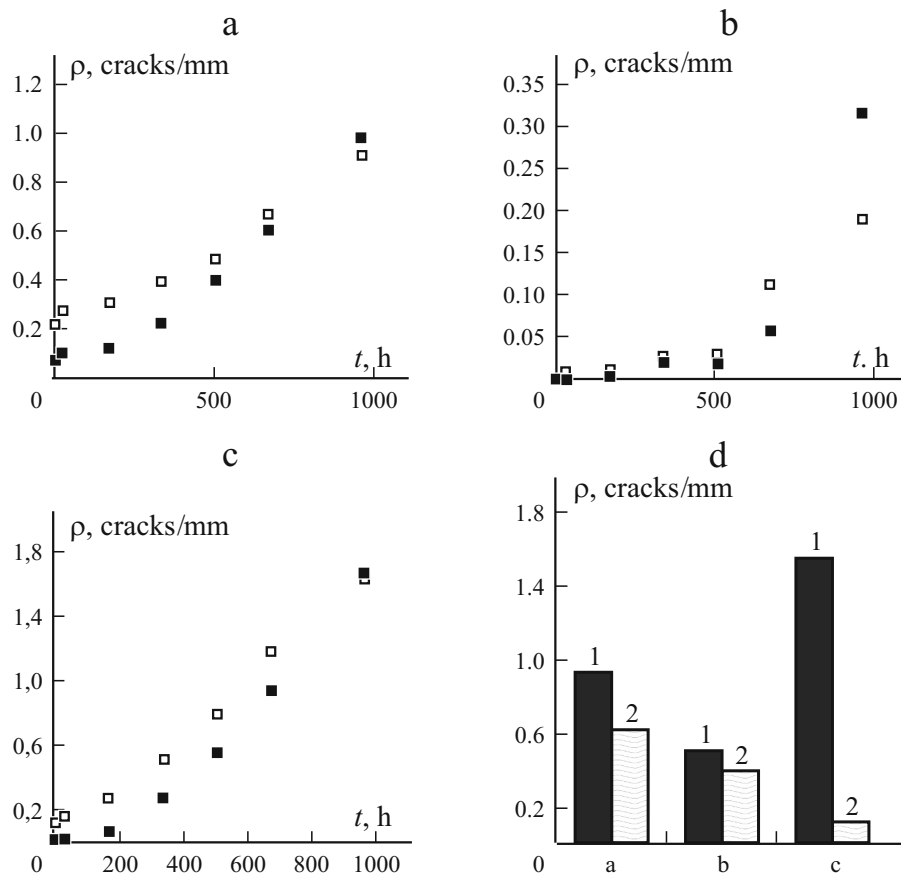
Fig. 2. Crack density ρ on the edge of the surface 45°-layers (a), internal 45°-layers (b), and 90°-layers (c) vs. aging hours (h) of specimens 432-4 (■) and 432-6 (□) and in the same layers of a 1000-h-aged A-432-2 specimen vs. the distances $d = 0$ (1) and 1.55 mm (2) from the edge (d).

In the middle part of the 90°- and internal 45°-layers, the value of $\Delta G = \Delta G_{90}$ was much greater than on the edge of the surface layer, and therefore, all initiated cracks in these layers had enough time to propagate through the middle part of the layer : indeed, the crack density there was very similar in the 90°- and 45°-layers. One could ask why the crack density at the edge of the 90°-layer was lower than in the middle part. There is no reason for that; we could even expect an opposite trend. Therefore, the differences in crack density in different locations of the 90°-layer can be used to estimate the scatter of data.

3.3. Thermal aging test

Specimens were exposed to 288°C in an ambient air environment for a certain time and then cooled down to RT to count cracks on specimen edges. The time at the high temperature reduced the characteristics of transverse failure of composite, and the thermal stresses at RT introduced new cracks. The crack density versus the number of aging hours is illustrated in Fig. 2. At the end of the test, the crack density in the surface +45°-layers was approximately 1crack/mm. Surprisingly, the crack density on the edge of the 90°-layer was higher than in the surface +45°-layer, reaching about 1.7 cracks/mm. The crack density at the edge of the internal ±45°-layers (the average over all layers) increased slower.

Figure 3 shows a fragment of the edge of a specimen before the thermal treatment (a) and after 40 days at 288°C (b). The matrix in the resin-rich regions had turned into calx and even fallen out. The cracks existing before the treatment had
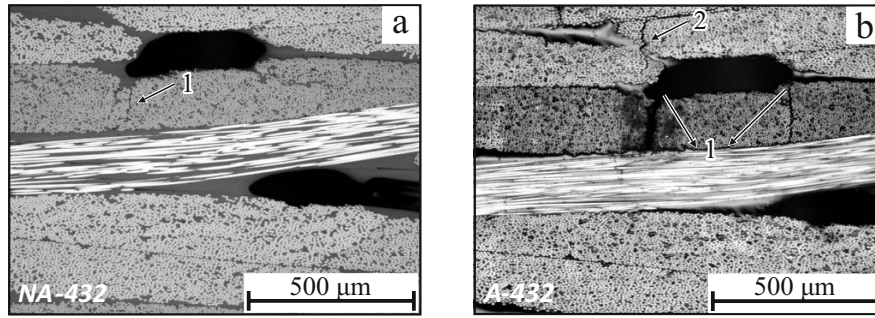
Fig. 3. Edge view of a specimen before (a) and after (b) a thermal exposure for 40 days at 288°C.
1 — crack in the 90° layer; 2 — crack in the –45° layer.

become much greater, because the treatment had damaged crack surfaces, the color of the edge had changed, and news cracks had appeared after cooling down to RT.

Edge polishing of the 40-day-aged specimen A-432-2 was performed to clarify whether the data on edge crack density were representative for the bulk of the composite. The results obtained, see Fig. 2d, show that, in the 90°-layer, the number of cracks away from the edge was much smaller and was very similar to that on the edge of the same specimen before aging. This indicates that, in the middle part of the 90°-layer, the material aging, due to the high-temperature exposure for 40 days, was rather small: the cracks initiated on the aged edge did not propagate into the layer.

During the aging test, the surface 45°-layers were in contact with the air environment over the whole surface. Therefore, more uniform (not only at the edge) material degradation can be expected in these layers, leading to an overall decrease in the resistance to crack initiation and propagation. The stresses at the edge of surface layers after aging were as low as the stresses in the internal 45°-layers, but the available energy conditions were more favorable for a crack to reach the edge.

The crack density on the edge of the internal 45°-layers was much lower than on the edge of the 90°-layers. This has a simple explanation: even if the material on the specimen edge was significantly degraded, the transverse stress in the 45°-layers at the edge was only 30% of that in the 90°-layers. Apparently, it was not sufficient to initiate new cracks. Regarding crack initiation in the middle part of the internal 45°-layers, there is a reason to assume that, similarly to that of the 90°-layers, the transverse failure resistance in the 45°-layers was not affected by temperature exposure. As a result, the crack density in the internal 45°-layers should be very similar to that in the 90°-layers. Still, Fig. 2d shows that it was higher than in the 90°-layers. This was because the data presented are the average over all internal 45°-layers. The aged zone propagated in the thickness direction from the specimen surface, and the crack density in the internal 45°-layers depended on the position of this layer with respect to the surface. The crack density in the 45°-layer next to the surface layer was much higher than in the 45°-layers close to the symmetry plane of the laminate, where the crack density was very similar to that in the 90°-layers. Obviously, aged had not only the surface layer, but also the next one, which was expected, because the thickness of one layer (0.18 mm) was much smaller that the size of the observed highly aged zone at the specimen edge (about 1 mm), even if the diffusion rate of oxygen had been higher in the fiber direction.

3.4. Damage development in a mechanical tensile loading

3.4.1. Observations and a Weibull analysis. Since the edge zone of the aged specimens was severely damaged, this zone was removed by polishing before the mechanical testing. Based on the results in Sect. 3.3, the degrading effect of thermal aging on the cracking resistance was expected mainly in the surface layers and much smaller, or even negligible, in the internal layers. The mechanical uniaxial tensile loading introduced more cracks, and delaminations were also observed between layers. The multiple cracking results presented below are based only on edge observations. To prove that the edge data were representative, the damage statistics on the edge was compared with the damage state quantified (after polishing) at several
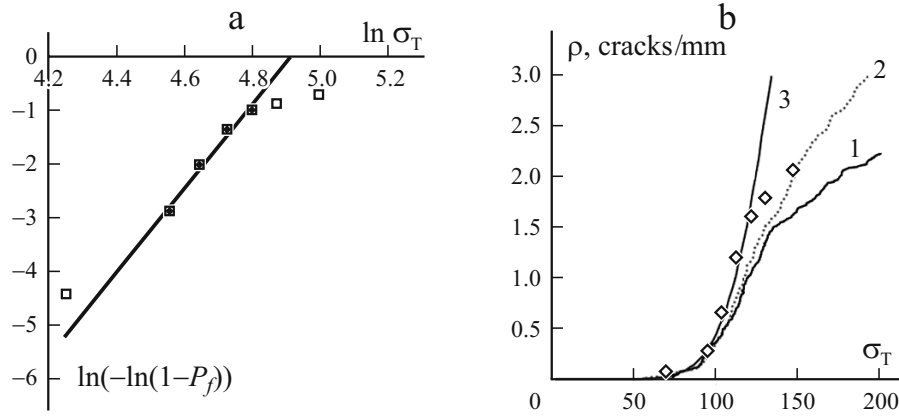
Fig. 4. Cracking in the 90°-layers (NA-432): experimental data (□) (a) and the linear fitting according to Weibull (——) (b); crack density ρ vs. the transverse stress σ_T according to the Hashin (1), the shear lag theory (2), and the P_f approaches (3); ◊ — experimental data (b).

distances from the edge by using one nonaged (NA) specimen after its loading to a 1% strain and one aged (A) specimen after its loading to a 0.7% strain. There was no statistically confirmed trend with more cracks on the edge of the specimen. The interlayer delaminations, usually starting from cracks, were measured finding that the fraction of the delaminated area was greater closer to the laminate surface. However, already at $d = 0.5$ mm from the edge, the delaminations were much smaller and they practically disappeared at $d = 1.5$ mm. Edge delaminations reduce stress concentrations at specimen edges and diminish the probability that a crack starts from the edge. The results presented give sufficient confidence in the ability of edge observations to represent the damage state of the entire laminate and in the suitability of the analysis presented in the next section. The observed independence of crack density on the distance from the edge means that most of the initiated cracks had enough ERR to propagate along the fiber direction and that the crack initiation stress should be used as the parameter to describe cracking in the composite. The following analysis is based on the stresses in the middle of specimen estimated using the CLT and not on edge stresses.

During the tensile test, thermal stresses did not change (the shear stress is zero), and the mechanical stresses in layers were proportional to the strain applied. For example, according to the CLT, at a 1% strain, the total transverse stress/shear stress ratio in the 45°-layer is $\sigma_{LT}^{45}/\sigma_T^{45} \approx 0.45$ (at a lower strain, the fraction of the shear stress is even lower). For this reason and knowing that the resistance to the shear cracking in composites is higher, we will neglect the contribution of shear stress to the failure criterion for a layer. The presence of shear stress could slightly increase the crack density.

The data on the crack density versus applied strain for the 90°-layer were "translated" to the relationship between the probability of failure P_f and the transverse stress σ_T in the layer. Equation (4) was used to calculate the probability of failure, and the CLT was used to calculate the thermomechanical stress in the 90°-layer of the quasi-isotropic laminate. If the Weibull distribution for the given material is valid, the experimental relationship obtained should follow Eq. (2) with $k = 1$ (internal layer). This routine is named the P_f-approach.

Following the standard procedure we plot $\ln(-\ln(1 - P_f))$ versus $\ln(\sigma_T)$, which, speaking theoretically, should be a linear relationship, from which the Weibull parameters can be obtained using a linear fitting. The values of the parameters obtained were as follows: $m = 7.84$ and $\sigma_{in0} = 135.2$ for the 432-NA composite and $m = 6.88$ and $\sigma_{in0} = 134.0$ for the 432-A one. The fitting result, see Fig. 4a, was rather sensitive to the data points used on both extremes: the points at high crack density were affected by stress perturbations from the neighboring cracks (the actual stress was lower than σ_T), whereas the stress on the rise of a first crack varied greatly from specimen to specimen, requiring a great number of specimens to be reliable.

The estimates of Weibull parameters obtained can be used in the more accurate Monte Carlo simulations over the whole crack density region and adjusted, if necessary, to increase the accuracy. Monte Carlo simulations require a stress analysis at any fixed damage state with a given spatial distribution of cracks. The stress distribution can be calculated using analyti-
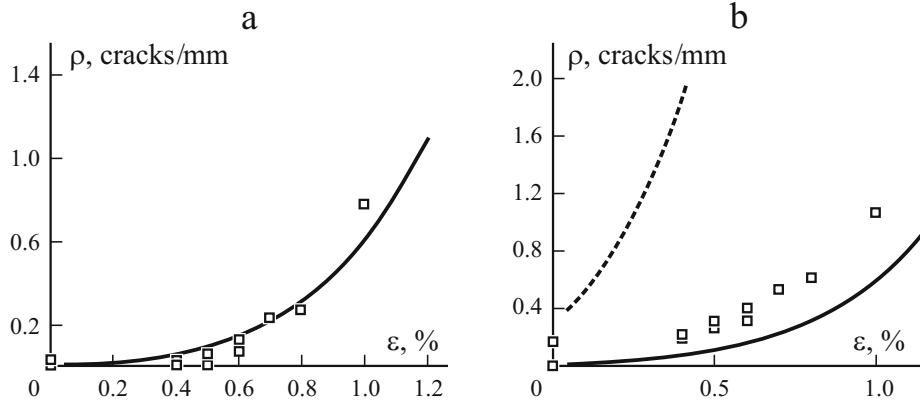
Fig. 5. Crack density ρ vs. applied strain ε in the internal (a) and surface +45°-layers of the NA-432 composite: experimental data ($\square$) and predictions of the P_f-approach at $k = 1$ (———) and $1.12\sqrt{2}$ (– – –).

cal models (the shear lag, Hashin, etc. ones). In each element of a layer, the parameter called the "failure index" (defined as the stress in the element versus its strength) is calculated to find the position of the next crack and the stress level. Then, the new crack is introduced, and the procedure is repeated. This procedure seems rather complex, but in this way, the interaction between cracks, which weakens the stress field and delays cracking, is considered.

3.4.2. Damage accumulation analysis. The ln–ln relationship for the 90°-layers in NA specimens is shown in Fig. 4a. Each data point is the average of all 90°-layers in three specimens. The first point on the left corresponds to the crack density caused by thermal stresses, which have a rather uncertain value. The last three points deviate from linearity, which is a sign of crack interaction. The data points used to determine Weibull parameters are indicated with filled symbols. According to Fig. 4b, where test data and the P_f-approach simulation using Eqs. (2) and (4) are shown, deviations start at $\rho_{90} \approx$ 1.6 cracks/mm. In general, the Weibull parameters obtained, together with Eqs. (2) and (4), give an acceptable description of cracking development. Monte Carlo simulations using the same Weibull parameters and two stress models between cracks (the shear lag model with a resin-rich layer of thickness $d_0 = 0.02$ mm and the Hashin model) are also shown: the Hashin model overestimated the crack interaction, but the shear lag model gave a good description for this rather arbitrarily selected value of the parameter d_0.

The Weibull parameters found from an analysis of the 90°-layer (see Sect. 3.4.1) were used to predict the crack density in the internal +45°-layers and in the surface +45°-layer of the NA laminate. All internal +45°-layers behaved in a very similar way, and presented are the average data. The data and simulations using the P_f-approach are illustrated in Fig. 5a, which shows a good agreement proving that a) cracking in the +45°-layers depends on the transverse stress in the same way as in the 90°-layers; b) at least for low loads, the effect of shear stresses in cracking simulation in the 45°-layers can be neglected. At low strains, the predicted crack density in the +45°-layers was slightly higher than the experimental, which can be attributed to an "imperfect" determination of parameters in the 90°-layer. Inclusion of shear stresses in the failure analysis (2) would not improve this agreement.

The crack density in the surface +45°-layer, which is shown in Fig. 5b, was significantly higher. The P_f-approach with $k = 1$ gave the same prediction as for the internal +45°-layers. An attempt to use Eq. (2) with $k = 1.12\sqrt{2}$ in simulations failed — a far too high crack density was predicted, see Fig. 5b. These results show that the discussion in Sect. 3.1 regarding the role of the free surface on defect growth has been oversimplified. In fact, the value of $k = 1.12\sqrt{2}$ was found to be right by computation micromechanics simulations only for the first crack [18]. It is not correct to assume that, in the surface layer of a laminate, all cracks will initiate at the free surface: even assuming that the defect state is uniform across the layer (it is just an assumption — in reality, there could be a resin-rich region at the surface changing the statistics), only the first cracks will originate from the largest defects close to the surface, but thereafter, the largest remaining defects will not be on the surface of the layer, and sooner or later, it will be their turn to grow. Thus, the multiple crack initiation in the surface layer should be a mix of cracks coming from the surface and from the interior of the layer.
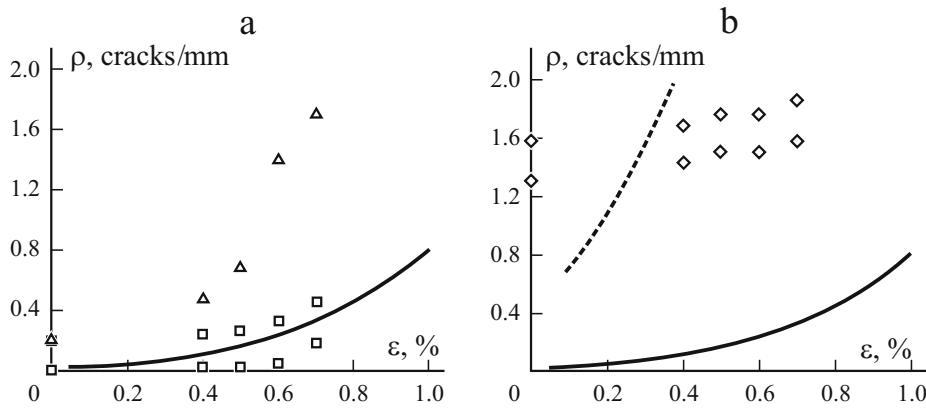
Fig. 6. Microcracking in the 90°- and internal 45°layers (a) and surface 45°-layers of the A-432 composite (b): predictions of the P_f-approach at $k = 1$ (——) and $1.12\sqrt{2}$ (– – –) and experimental data for 90°- ($\triangle$), internal 45°- ($\square$), and surface 45°-layers ($\lozenge$).
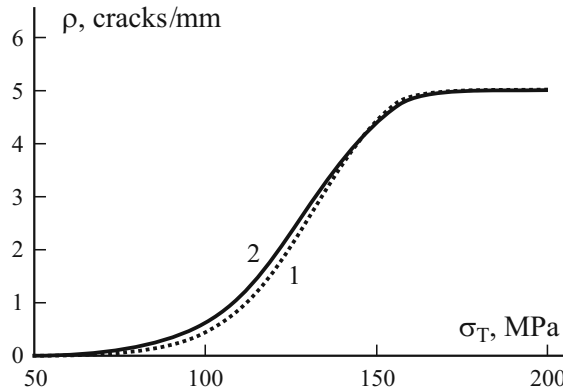

Fig. 7. Simulated intralaminar crack density curves in the 90°-layers of nonaged (1) and thermally aged (2) specimens according to the P_f-approach.

3.4.1. Effect of aging on the damage development in tension. The Weibull parameters for the A-432 specimens (see Sect. 3.4.1) obtained from cracking data in the 90°-layers were used in the P_f-approach to predict the crack density growth in the 45°-layers, see Fig. 6. For the internal +45°-layers, predictions were in good agreement with test data.

Just as for the NA specimens, the crack density in the surface layers could not be predicted: it was even outside the previously discussed bounds with two values of k. The latter means that the surface layer had different failure properties than the internal layers: it has aged (a lower fracture toughness and/or initiation stress), and therefore ρ was much higher than in the internal 90°-layers.

The probability of transverse failure in the 90°-layers (nonaged and aged) was very similar: the high-temperature exposure had not affected their damage behavior. Crack density simulations for the 90°-layers of aged and nonaged plates using the data given in Sect. 3.4.1 are shown in Fig. 7.

3.4.4. Extraordinary cracking pattern in the –45°-layers. In the nondamaged quasi-isotropic $[(+45/–45)/(90/0)]_{2s}$ laminate, the CLT stresses in the ±45°-layers were exactly the same, and, therefore, the same development of multiple cracking could be expected in both the types of layers. Nevertheless, the data presented in Fig. 7a show much more cracks in the internal –45°-layers than in the internal +45°-layers.

In these figures, the P_f-approach simulations, which describe cracking in the +45°-layers very well, are shown by the solid lines. The crack density is shown separately in the L3 –45°-layer, which is close to the midplane, and in the L7 –45°-layer,
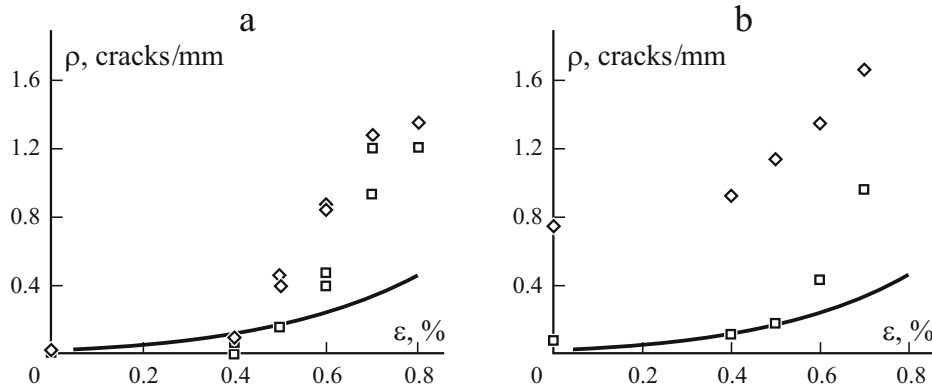
Fig. 8. Cracking in the –45°-layers of nonaged (a) and aged (b) 432 quasi-isotropic laminates: experimental data for the L3 (□) and L7 (◇) layers and prediction of the P_f-approach at $k = 1$ (——).

which is close to the surface (next to the surface layer). At a 0.6% strain, the crack density in –45°-layers of the nonaged specimen was almost two times higher than in the +45°-layers of the same specimen. The only explanation for the systematically higher crack density in the –45°-layers is the stress concentrations due to the damage developing in the neighboring layers. An internal +45°-layer had 0°- and –45°-layers as adjacent ones. There were no cracks in the 0°-layers (except some thermal cracks). The cracks in the adjacent –45°-layer were oriented perpendicularly to the transverse direction of the +45°-layer, and therefore, the stress concentrations in it had a rather small effect on cracking in the +45°-layer. In contrary, the –45°-layer was surrounded by a +45°-layer (the same marginal effect from cracks in this layer) and a 90°-layer, where the crack density increased faster than in the other ones. The cracks in the 90°-layers caused larger regions of strong concentrations of transverse stress in the adjacent –45°-layer, leading to cracks of small length, often called stitch cracks, owing to their appearance. They have been observed in both the mechanical and thermal fatigue and also in quasi-static loadings [2, 19]. If the crack propagation stress is low, the stich cracks grow along fibers across the whole width of specimen.

In the nonaged specimens (Fig. 7a), the crack density in the L3 layer was only slightly lower than in the L7 one. In the aged specimens (Fig. 7b), the difference was striking: a much higher crack density was in the L7 layers. In the L3 layers, the cracking was similar both in nonaged and aged specimens. An obvious explanation for that is aging: the layers close to the laminate midplane had nonaged. Aged had only the surface layer and the L7 –45°-layer.

4. Conclusions

The intralaminar cracking in a quasi-isotropic CF/polyimide 8-harness satin composite was investigated. Fractography was used to analyze the initial damage state of the composite after manufacturing and its change owing to exposure to 288°C for 40 days, thermal cycling, and tensile loading.

Analyzing the initial damage in nonaged specimens and its development in thermal cycling, a much faster growth in crack density was found in the surface layers because of the free-surface effect on the initiation and propagation of intralaminar cracks.

The degradation of composite with time during a high-temperature exposure was determined interrupting the treatment after a certain time, bringing specimens to room temperature, and counting cracks. The greatest increase in crack density was observed in the surface layers. In the internal layers (especially in the 90°-layers), only about 1mm of the edge zone was degraded, but inside the material, the crack density was statistically the same as before the temperature exposure.

In the tensile loading, the crack density in different layers of the laminate was quantified and analyzed using the Weibull distribution of transverse strength for crack initiation. A simplified method to determine the Weibull parameters and a cracking simulation scheme neglecting crack interaction were used to compare aged and nonaged materials. It was found that cracking in the internal +45°-layers could be predicted based on the Weibull properties of the 90°-layers. The crack density

in the surface +45°-layer was much higher even for nonaged specimens, which can be explained by the free-surface effect on crack initiation. The thermal treatment significantly reduced the resistance of the surface layer to cracking in mechanical tension. Degraded not only the surface layer, but also the layer next to it, whereas, the failure resistance of central layers was not affected. Cracking in the 45°-layers adjacent to the 90°-layer was significantly accelerated by stress concentrations from the cracks in the 90°-layer.

REFERENCES

1. G. A. Owens and S. E. Schofield, "Thermal cycling and mechanical properties assessment of carbon fiber fabric reinforced PMR-15 polyimide laminates," Compos. Sci. Technol., **33**, 177-190 (1988),

2. V. T. Bechel, M. Negilski, and J. James, "Limiting the permeability of composites for cryogenic applications," Compos. Sci. Technol., **66**, No. 13, 2284-2295 (2006).

3. T. K. Tsotsis, S. Keller, K. Lee, J. Bardis, and J. Bish, "Aging of polymeric composite specimens for 5000 hours at elevated pressure and temperature," Compos. Sci. Technol., **61**, 75-86 (2001).

4. K. Giannadakis and J. Varna, "Effect of thermal aging and fatigue on failure resistance of aerospace composite materials," IOP Conf. Series: Materials Science and Engineering 5, (2009).

5. V. T. Bechel, J. D. Camping, and R. Y. Kim, "Cryogenic /elevated temperature cycling induced leakage paths in PMCs," Composites: Part B, **36**, 171-182 (2005).

6. D. E. Bowles and J. Shen, "Thermal cycling effects on the dimensional stability of P75 and P75-T300(Fabric) hybrid graphite/epoxy laminates," 33rd Int. SAMPE Symp., 1988

7. D. Lévêque, A. Schieffer, A. Mavel, and J. F. Maire, "Analysis of how thermal aging affects the long-term mechanical behavior and strength of polymer-matrix composites," Compos. Sci. Technol., **65**, 395-401 (2005).

8. C. Marceau and B. Hilaire, "Thermal ageing of PMR15 polyimide matrix," Polymer, **34**, 2458-2459 (1993).

9. P. D. Mangalgiri, "Polymer-matrix composites for high-temperature applications," Defense Sci. J., 55, 175-193 (2005).

10. S. A. Tsampas, P. S. Fernberg, and R. Joffe, "Mechanical performance of novel high Tg polyimide matrix carbon fiber-reinforced laminates," 20th Int. Conf. on Composite Materials, Copenhagen, 19-24 July 2015

11. J. Varna, R. Joffe, L. A. Berglund, and S. Lundström, "Effects of voids on failure mechanisms in RTM laminates," J. Composite Sci. Technol., **53**, 241-249 (1995).

12. S. Sisodia, E. K. Gamstedt, F. Edgren, and J. Varna, "Effects of voids on quasi-static and tension fatigue behaviour of carbon-fiber composite laminates," J. of Composite Materials, **49**, No. 17, 2137-2148 (2015).

13. D. Broek, Elementary Engineering Fracture Mechanics, Sijtholf & Noordhoff, Alpena an den Rijn, The Netherlands, 1978

14. L. A. Berglund, J. Varna, and J. Yuan, "Transverse cracking and local delamination in [04/90n]S and [90n/04]S carbon fiber/toughened epoxy laminates," J. Reinforced Plastics and Composites, **11**, 643-660 (1992).

15. J. Varna, "Modeling mechanical performance of damaged laminates," J. of Composite Materials, **47**, No. 20-21, 2443-2474 (2013).

16. M. Quaresimin, P. A. Carraro, L. P. Mikkelsen, N. Lucato, L. Vivian, P. Brøndsted, B.F. Sørensen, J. Varna, and R. Talreja, "Damage evolution under cyclic multiaxial stress state: A comparative analysis between glass/epoxy laminates and tubes," Composites: Part B: Engineering, **61**, 282-290 (2014).

17. V. T. Bechel, "Permeability and damage in unloaded cryogenically cycled PMCs," 46th AIAA/ASME/ASCE/AHS/ASC Structures, Structural Dynamics and Materials Conf.,18-21 April 2005, Austin, Texas

18. M. Herraez, D. Mora, F. Naya, C. S. Lopes, C. Gonzales; and J. LLorca, "Transverse cracking of cross-ply laminates: A computational micromechanics perspective," Compos. Sci. Technol., **110**, 196-204 (2015).

19. M Loukil, Z. Ayadi, and J. Varna, "ESPI analysis of crack face displacements in damaged laminates," J. Compos. Sci and Technol., **94**, No. 9, 80-88 (2014).